Bifurcation Transition and Nonlinear Response in a Fractional-Order System

J. H. Yang[1]
School of Mechatronic Engineering,
China University of Mining and Technology,
Xuzhou 221116, China
e-mail: jianhuayang@cumt.edu.cn

M. A. F. Sanjuán
Nonlinear Dynamics, Chaos, and Complex
Systems Group,
Departamento de Física,
Universidad Rey Juan Carlos,
Tulipán s/n,
Móstoles, Madrid 28933, Spain
e-mail: miguel.sanjuan@urjc.es

H. G. Liu
School of Mechatronic Engineering,
China University of Mining and Technology,
Xuzhou 221116, China

G. Cheng
School of Mechatronic Engineering,
China University of Mining and Technology,
Xuzhou 221116, China

We extend a typical system that possesses a transcritical bifurcation to a fractional-order version. The bifurcation and the resonance phenomenon in the considered system are investigated by both analytical and numerical methods. In the absence of external excitations or simply considering only one low-frequency excitation, the system parameter induces a continuous transcritical bifurcation. When both low- and high-frequency forces are acting, the high-frequency force has a biasing effect and it makes the continuous transcritical bifurcation transit to a discontinuous saddle-node bifurcation. For this case, the system parameter, the high-frequency force, and the fractional-order have effects on the saddle-node bifurcation. The system parameter induces twice a saddle-node bifurcation. The amplitude of the high-frequency force and the fractional-order induce only once a saddle-node bifurcation in the subcritical and the supercritical case, respectively. The system presents a nonlinear response to the low-frequency force. The system parameter and the low-frequency can induce a resonance-like behavior, though the high-frequency force and the fractional-order cannot induce it. We believe that the results of this paper might contribute to a better understanding of the bifurcation and resonance in the excited fractional-order system. [DOI: 10.1115/1.4029512]

Keywords: fractional-order calculus, transcritical bifurcation, saddle-node bifurcation, resonance

1 Introduction

Bifurcation analysis is important in the engineering and scientific fields. Bifurcations may make the system to lose stability and results in disasters in some cases. Recently, the bifurcation in fractional-order systems has attracted more and more attention. This is because the fractional-order calculus is a powerful tool for modeling properties of some special materials, such as Newtonian fluids [1], viscoplasticity [2], viscoelasticity [3,4], rheology [5,6], etc. There are lots of publications concerning bifurcations in fractional-order systems. For example, in discrete fractional maps, the bifurcation will occur and usually leads to chaos [7–9]. In a single force excited Duffing oscillator, the period doubling bifurcation appears [10,11]. In the double forces excited, fractional-order Duffing oscillator [12] and quintic oscillator [13], the pitchfork bifurcation can be induced by the high-frequency excitation. In the fractional-order nonautonomous system [14], the delay fractional-order system [15], and the fractional-order modified hybrid optical system [16], the Hopf bifurcation happens. In a simplified Lorenz system, the period doubling bifurcation, the flip bifurcation, the tangent bifurcation, and the interior crisis bifurcation are observed [17], just to mention a few examples.

The normal form of a transcritical bifurcation is given by

$$\frac{dx}{dt} = \mu x - x^2 \qquad (1)$$

where μ is a real parameter [18–20]. When the parameter μ changes from negative to positive, the transcritical bifurcation occurs. The potential function of Eq. (1) is $U(x) = -(1/2)\mu x^2 + (1/3)x^3$. This potential function can model the potential energy of some supporting structures in engineering. As described in the first paragraph, if the structure frame is comprised by some special materials, it might be much more reasonable to model the structure by the fractional calculus. Given these considerations, we proceed to rewrite Eq. (1) in a general fractional-order version, i.e.,

$$\frac{d^\alpha x}{dt^\alpha} = \mu x - x^2 \qquad (2)$$

Further, in many engineering backgrounds, the structure is usually excited by a harmonic force or the combination of both a low- and a high-frequency force [19,21,22]. Taking into account all these factors, we finally consider the fractional-order system excited by both a low- and a high-frequency force

$$\frac{d^\alpha x}{dt^\alpha} = \mu x - x^2 + f\cos(\omega t) + F\cos(\Omega t) \qquad (3)$$

Here, α denotes the order of the fractional derivative. In general, $0 < \alpha < 2$. There are three definitions often used in describing the fractional-order derivative, i.e., the Riemann–Liouville definition, the Caputo definition and the Grünwald–Letnikov definition [23]. Herein, we adopt the Grünwald–Letnikov definition for its widely used and simplicity in the numerical discretization. The Grünwald–Letnikov definition is defined as

$$\frac{d^\alpha x(t)}{dt^\alpha}\Big|_{t=kh} = \lim_{h \to 0} \frac{1}{h^\alpha} \sum_{j=0}^{k} (-1)^j \binom{\alpha}{j} x(kh - jh) \qquad (4)$$

where the binominal coefficients are

$$\binom{\alpha}{0} = 1, \quad \binom{\alpha}{j} = \frac{\alpha(\alpha-1)\cdots(\alpha-j+1)}{j!}, \text{for } j \geq 1 \qquad (5)$$

The two forces in the excitations are a low- force and a high-frequency force, respectively, i.e., $\omega \ll \Omega$. The high-frequency

force in a nonlinear system usually has the effects of stiffening, biasing, and smoothening [19,24]. In a symmetric bistable system, the high-frequency force induces a pitchfork bifurcation due to its stiffening effect on the system [12]. In an asymmetric bistable system, the high-frequency force has both the stiffening and the biasing effects. It induces a saddle-node bifurcation [25]. In fact, if the symmetric or asymmetric bistable system is not excited by the two-frequency forces, the pitchfork bifurcation or the saddle-node bifurcation also appears, respectively, by changing the system parameter. In other words, the system posses the bifurcation inherently. However, the present system is different from a bistable system. It is monostable with one stable and one unstable equilibrium when $\mu \neq 0$. To the best of our knowledge, the effect of the high-frequency force in the system of this kind has not been reported elsewhere. In addition, the various bifurcation behaviors of this system under different excitations have not been investigated yet. Further, the nonlinear response of the considered system is another concern. These problems are the main motivations of this paper.

The outline of the present work is organized as follows. In Sec. 2, when the system is excited by the low-frequency force only, the transcritical bifurcation is briefly studied. In Sec. 3, when the system is excited by both the low- and the high-frequency forces, we find that the transcritical bifurcation transits to the saddle-node bifurcation. Then, the effects of the system parameter, the high-frequency force and the fractional-order on the saddle-node bifurcation are discussed by both analytical and numerical methods. In Sec. 4, the nonlinear response of the system to the low-frequency force is investigated. Finally, the work is concluded in the last section.

2 Transcritical Bifurcation

The transcritical bifurcation is a typical local codimension-one bifurcation for flows. At a point of a transcritical bifurcation, two equilibrium solutions meet and exchange stability. The bifurcation is continuous because there is a continuous path on the stable branch through the bifurcation point in the bifurcation diagram. To investigate the local bifurcation, the equilibrium solutions of the excitation-free system should be computed. Apparently, the equilibrium points of Eq. (1) or Eq. (2) are $x = 0$ and $x = \mu$ for any α. As shown in Fig. 1, if $\mu < 0$, the line $x = 0$ is the stable equilibrium branch; if $\mu > 0$, the line $x = \mu$ is the stable equilibrium branch. The critical value $\mu = 0$ is the bifurcation point at which the stability of the equilibriums of the two branches exchanges. As it has been mentioned above, the bifurcation diagram of this kind are given in many monographs [18–20].

When the excitation is absent, and under some different initial conditions, the response of the system may be convergent to the
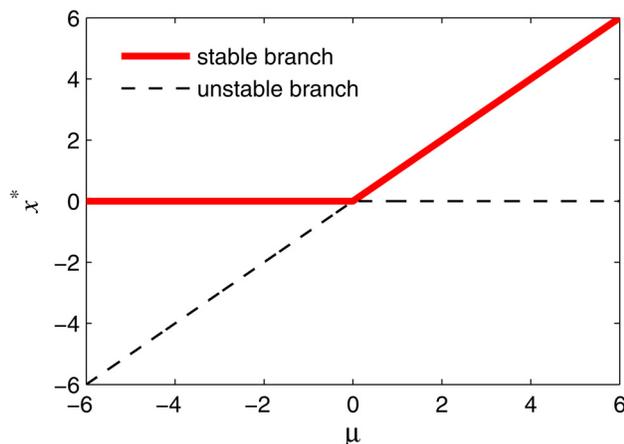

Fig. 1 The system parameter μ induced transcritical bifurcation diagram for system (1) and system (2)

stable equilibrium with the increase of time. If the system is excited by the external force, the response of the system may move around the stable equilibrium. Certainly, if the excitation is strong enough, the response will diverge to infinity when the portraits approach to the unstable manifold. In Fig. 2, the phase trajectories under different parameters are shown. We let $F = 0$ in this figure. In other words, only the low-frequency force is considered. If $\mu < 0$, the phase trajectories move around the stable equilibrium $x = 0$, as shown in Figs. 2(a), 2(c), and 2(e). If $\mu < 0$, the phase trajectories move around the stable equilibrium $x = \mu$, as shown in Figs. 2(b), 2(d), and 2(f). The phase trajectories are not divergent and move around the sole stable equilibrium in these subplots. The value of the fractional-order does not influence the location of the stable equilibrium. In this figure, the transcritical bifurcation occurs when the system parameter μ varies from -4 to 4. Hence, Figs. 1 and 2 carry the same information on the transcritical bifurcation.

3 Saddle-Node Bifurcation

The saddle-node bifurcation is another typical local codimension-one bifurcation for flows. At a point of a saddle-node bifurcation, two equilibrium solutions coalesce and disappear/appear. The saddle-node bifurcation is said to be a discontinuous bifurcation because the bifurcation point corresponds to the starting point or the end point of the solution branches. Hence, the nature of the saddle-node bifurcation is different from the transcritical bifurcation. Further, the saddle-node bifurcation is stable, but the transcritical bifurcation is unstable to the polynomial perturbation [19]. Specifically, a polynomial perturbation will make the transcritical bifurcation disappear and a new type of bifurcation appear. However, under a polynomial perturbation, the saddle-node bifurcation is still of a saddle-node type. In the following analysis, we will see that the transcritical bifurcation is also unstable to the high-frequency force. The high-frequency force has the effect similar to the polynomial perturbation in the system and makes a transcritical bifurcation transit to a saddle-node bifurcation. The effects of the system parameter, the
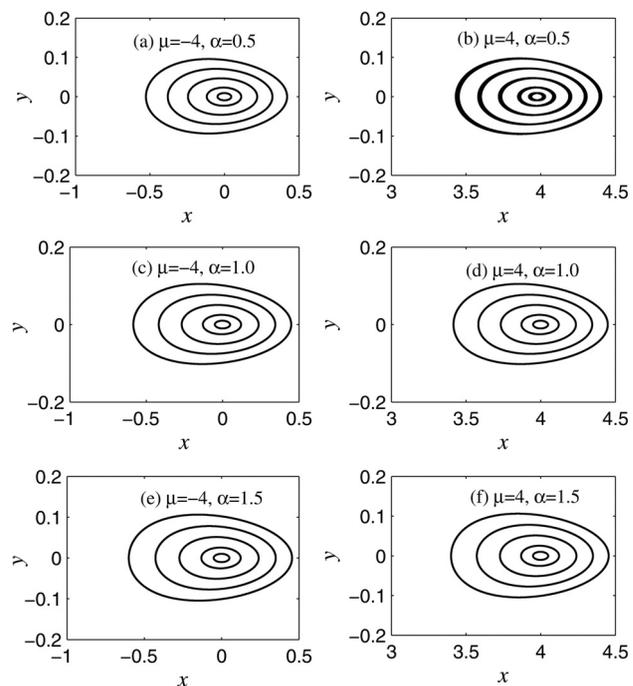

Fig. 2 Phase trajectories of system (3) under the excitation of the low-frequency force only. For numerical simulation, $y = dx/dt$, $F = 0$, $\omega = 0.2$, and $f = 0.2$, 0.5, 1.0, 1.5, and 2.0 from the inside to the outside in each subplot.

high-frequency force and the fractional-order on the saddle-node bifurcation will be studied in detail.

3.1 Theoretical Framework. To investigate the effects of the high-frequency force and the fractional-order on the local behavior in Eq. (3), we should eliminate the high-frequency force in the system at first. The method of direct separation of slow and fast motions is a useful tool in studying the system which is excited by both the low-frequency and the high-frequency forces. This method has been successfully used in different systems, such as in a friction system [26], a delayed system [27,28], a fractional-order system [29], a noisy system [30], a pendulum [31,32], beams [33], rotating disks [34], fluid pipes [21,35], etc. This method is much simpler than some other approximate methods in the linear response scope.

Due to the fact that $\omega \ll \Omega$ in Eq. (3), the method of separation of slow and fast motions can be used. Based on this method, we let $x = X + \Psi$. Here, X and Ψ are the slow and fast motions with period $2\pi/\omega$ and $2\pi/\Omega$, respectively. Substituting $x = X + \Psi$ into Eq. (3), we obtain

$$\frac{d^\alpha X}{dt^\alpha} + \frac{d^\alpha \Psi}{dt^\alpha} = \mu X + \mu \Psi - X^2 - 2X\Psi - \Psi^2 + f\cos(\omega t) + F\cos(\Omega t) \tag{6}$$

Searching an approximate solution of Ψ in the linear equation

$$\frac{d^\alpha \Psi}{dt^\alpha} = \mu \Psi + F\cos(\Omega t) \tag{7}$$

And solving Eq. (5), it is easy to obtain the solution of Ψ

$$\Psi = \frac{F}{\beta}\cos(\Omega t - \theta) \tag{8}$$

where

$$\begin{cases} \beta^2 = \left(\Omega^\alpha \cos\frac{\alpha\pi}{2} - \mu\right)^2 + \left(\Omega^\alpha \sin\frac{\alpha\pi}{2}\right)^2 \\ \theta = \tan^{-1}\dfrac{\Omega^\alpha \sin\dfrac{\alpha\pi}{2}}{\Omega^\alpha \cos\dfrac{\alpha\pi}{2} - \mu} \end{cases} \tag{9}$$

Substituting Eq. (8) into Eq. (6) and averaging all terms in the interval $[0, 2\pi/\Omega]$, we have the equation for the slow motion

$$\frac{d^\alpha X}{dt^\alpha} = \mu X - X^2 - \frac{F^2}{2\beta^2} + f\cos(\omega t) \tag{10}$$

Hereto, the fast motion disappears and only the slow motion is retained. Equation (10) apparently shows that $-F^2/2\beta^2$ is a constant term and has the biasing effect on the equivalent system. This term is a perturbation and will make the transcritical bifurcation transit to the saddle-node bifurcation. Hence, the high-frequency force has a biasing effect. It is a key factor in order to make the new type of bifurcation to appear. In addition, the effect of the high-frequency excitation on the system is different from that in the symmetric bistable system in which the stiffening effect is observed [12,36,37]. According to Eq. (10), the bifurcation can be investigated analytically. The equilibrium points of Eq. (10) are obtained by solving the equation

$$\mu X - X^2 - \frac{F^2}{2\beta^2} = 0 \tag{11}$$

If $\mu^2 - (2F^2/2\beta^2) \geq 0$, Eq. (10) has two equilibria

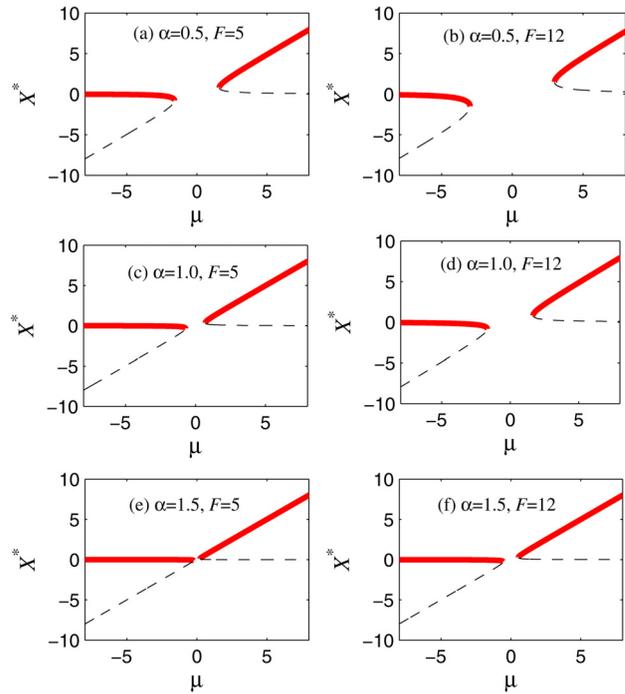$$X^*_{1,2} = \frac{\mu \pm \sqrt{\mu^2 - 2F^2/\beta^2}}{2} \tag{12}$$

Fig. 3 Analytical prediction of the saddle-node bifurcation that induced by the system parameter μ for $\Omega = 10$. The continuous thick lines are the stable branches and the dashed thin lines are the unstable branches.

Or else, Eq. (10) has no real root. One equilibrium point in Eq. (12) is stable. The other equilibrium point in Eq. (12) is unstable. The saddle-node bifurcation occurs when $\mu^2 = 2F^2/2\beta^2$.

In most cases, the response of the system to the low-frequency excitation deserves a particular concern. This is because the low-
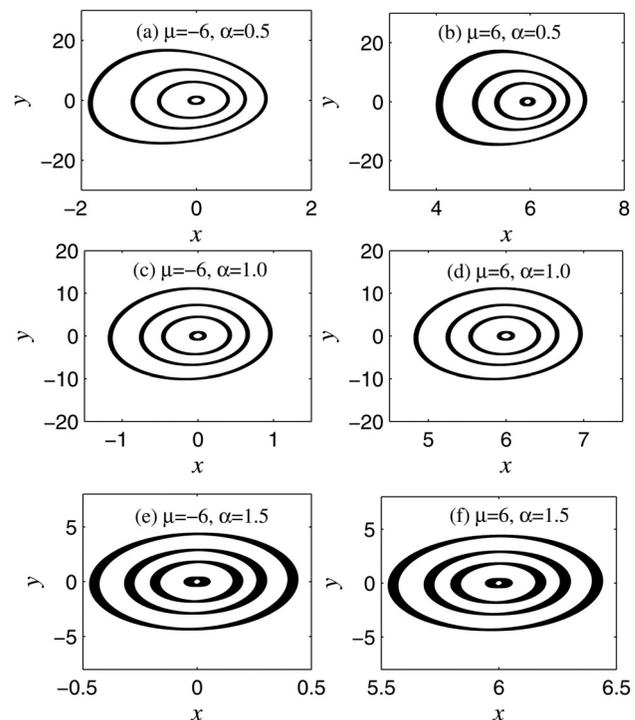

Fig. 4 Phase trajectories of system (3) under the excitation of the two harmonic forces. For numerical simulation, $y = dx/dt$, $f = 0.1$, $\omega = 1$, $\Omega = 10$, and $F = 1, 5, 8$, and 12 from the inside to the outside in each subplot.
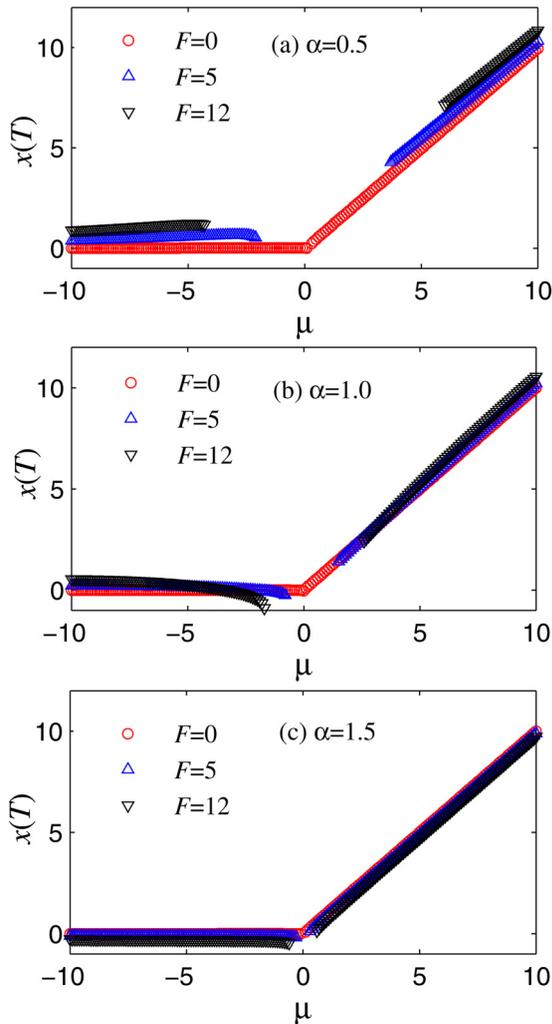
Fig. 5 Numerical prediction of the transcritical and saddle-node bifurcations that induced by the system parameter μ. The simulation parameters are $f = 0.01$, $\omega = 1$, and $\Omega = 10$.

frequency excitation may induce a catastrophe, even though it is very weak. To obtain the response at the low-frequency, we need to take away the constant component at first. Letting $Y = X - X^*$, where X^* is the stable equilibrium, then we obtain

$$\frac{d^\alpha Y}{dt^\alpha} = \omega_r Y - Y^2 + f\cos(\omega t) \tag{13}$$

Fig. 6 Analytical prediction of the saddle-node bifurcation that induced by the force amplitude F for $\Omega = 10$. The continuous thick lines are the stable branches and the dashed thin lines are the unstable branches.
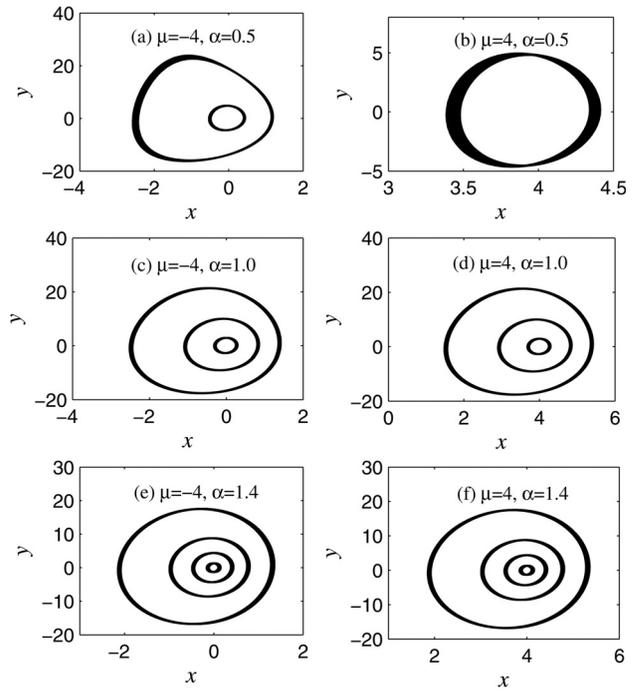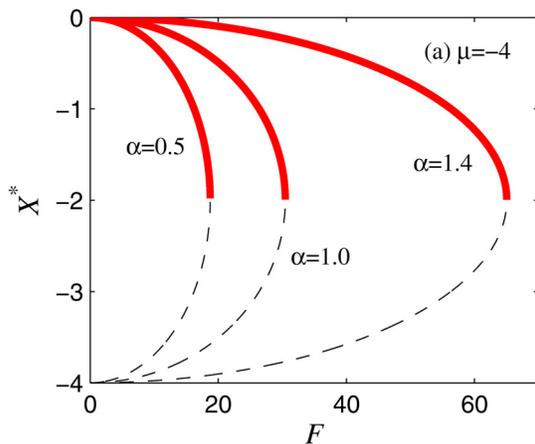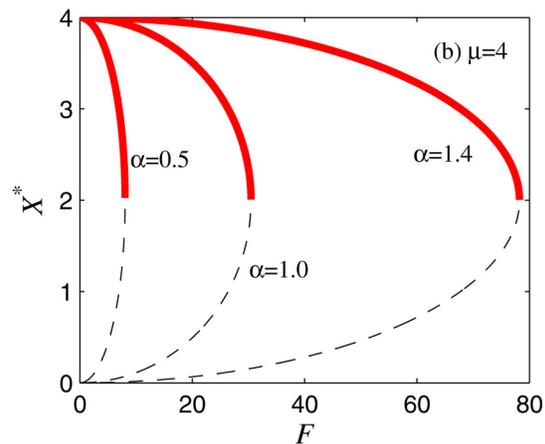

Fig. 7 Phase trajectories of system (3) under the excitation of the two harmonic forces. For numerical simulation, $y = dx/dt$, $f = 0.1$, $\omega = 1$, $\Omega = 10$, and $F = 3$, 10, 20, and 40 from the inside to the outside in each subplot. The phase trajectories are divergent when $F = 20$ and 40 in (a), $F = 10$, 20 and 40 in (b), $F = 40$ in (c) and (d).

where $\omega_r = \mu - 2X^*$. When $t \to +\infty$, the response of the system at the low-frequency ω can be obtained from the following linear equation

$$\frac{d^\alpha Y}{dt^\alpha} = \omega_r Y + f\cos(\omega t) \tag{14}$$

Solving Eq. (14), we obtain $Y = (f/\gamma)\cos(\omega t - \varphi)$ with

$$\begin{cases} \gamma^2 = \left(\omega^\alpha \cos\frac{\alpha\pi}{2} - \omega_r\right)^2 + \left(\omega^\alpha \sin\frac{\alpha\pi}{2}\right)^2 \\ \varphi = \tan^{-1}\dfrac{\omega^\alpha \sin\dfrac{\alpha\pi}{2}}{\omega^\alpha \cos\dfrac{\alpha\pi}{2} - \omega_r} \end{cases} \tag{15}$$

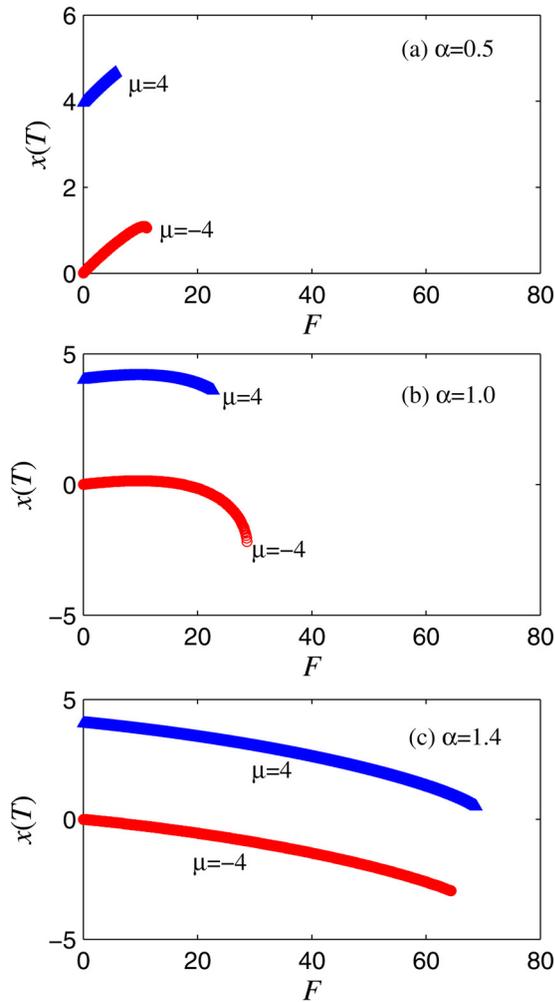The enhancement of the low-frequency force can be quantified by the response amplitude Q, which is defined by

Fig. 8 Numerical prediction of the saddle-node bifurcation that induced by the force amplitude *F*. The simulation parameters are *f* = 0.01, *ω* = 1, and Ω = 10.

$$Q = \frac{1}{\gamma} = \frac{1}{\sqrt{\left(\omega^\alpha \cos\frac{\alpha\pi}{2} - \omega_r\right)^2 + \left(\omega^\alpha \sin\frac{\alpha\pi}{2}\right)^2}} \quad (16)$$

The response amplitude of the system to the low-frequency excitation can be predicted, according to Eq. (16), by using the magnitude Q. Here, we must emphasize that the precondition for Eq. (16) is the existence of X^*. If X^* does not existence, the expression of Q in Eq. (16) is invalidity. The response will diverge to infinity for this case.

3.2 The System Parameter Induced Saddle-Node Bifurcation. When the high-frequency term is not included in the excitation, the system parameter μ induces a transcritical bifurcation, as shown in Fig. 1. However, when the system is excited by the two-frequency forces, the equivalent equilibria do not always exist according to Eq. (12). The equilibrium disappears when there are no real solutions for the Eq. (12). Hence, the transcritical bifurcation transits to the saddle-node bifurcation when the solution branches disappear. In Fig. 3, the system parameter μ induced saddle-node bifurcation is given according to the analytical prediction. There are two points of the saddle-node bifurcation in each subplot. The bifurcation point in the leftward is the end point of the two equilibrium branches. At this point, the stable branch and the unstable branch coalesce and disappear. The bifurcation point in the rightward is the beginning point of the two equilibrium branches. The stable branch and the unstable branch start at this point. There is a discontinuous interval between the two bifurcation points. It indicates that the response is divergent when μ lies in this interval. Further, from these subplots, we know that the space interval looks much wider when the value of α is small. The bifurcation diagram in Fig. 3 is naturally different from that in Fig. 1. The curve in Fig. 1 is the continuous transcritical bifurcation diagram. However, the curve in Fig. 3 is the discontinuous saddle-node bifurcation diagram. In a word, the high-frequency force causes a qualitative change to the bifurcation diagram in the considered system.

Under different simulation parameters, the phase trajectories are plotted in Fig. 4. In this figure, no matter the parameter μ is negative or positive, the phase trajectories move around the sole stable equilibrium. With the increase of the value of the fractional-order, the amplitude of the phase cycle turns smaller. As to the parameter F, it makes the response amplitude of the phase cycle turns larger with the increase of F. Under these simulation parameters, the stable equilibria are always existing according to Eq. (12) and Fig. 3. Hence, the phase trajectories are always existing too.

Besides the analytical prediction of the bifurcation in Fig. 3, the bifurcation diagram can also be obtained by numerical methods. We choose an initial condition to calculate the time series. If the stable equilibrium exists, the response will try to approach the
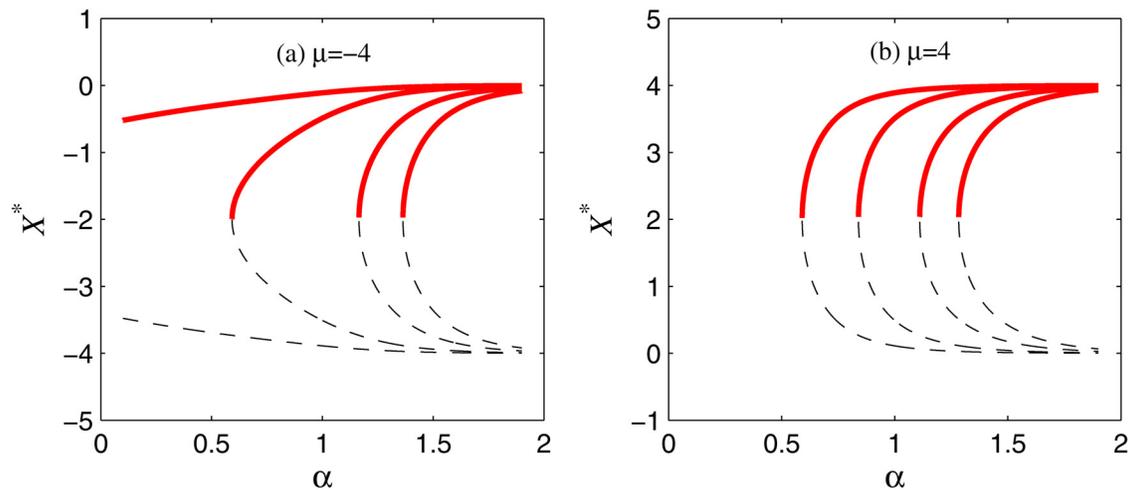

Fig. 9 Analytical prediction of the saddle-node bifurcation that induced by the fractional-order α. The continuous thick lines are the stable branches and the dashed thin lines are the unstable branches. The simulation parameters are Ω = 10 and *F* = 10, 20, 40, 60 from the left curve to the right curve in each subplot.
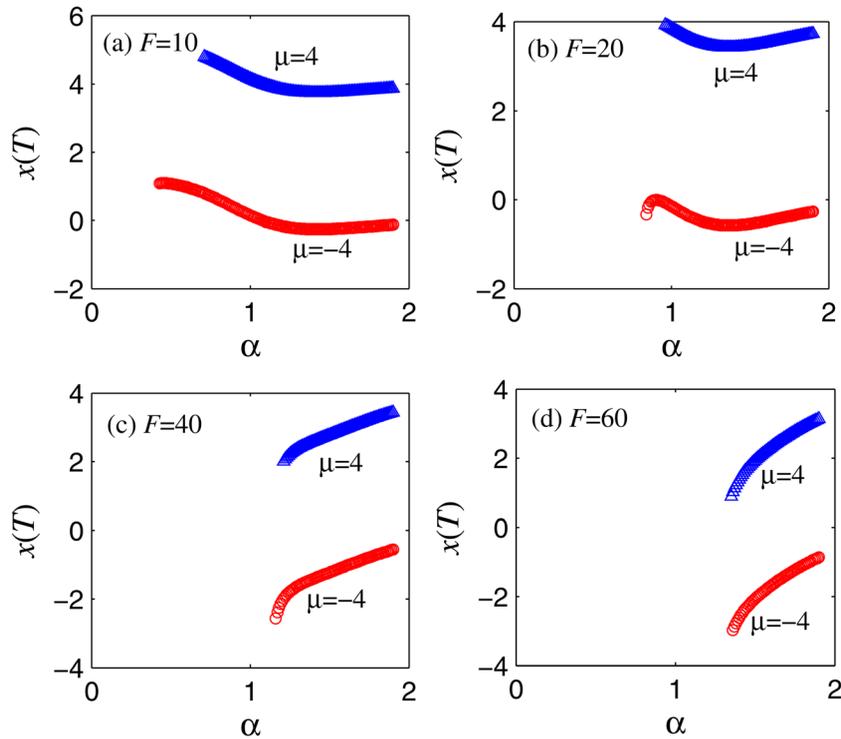
Fig. 10 Numerical prediction of the saddle-node bifurcation that induced by the fractional-order α. The simulation parameters are $f = 0.01$, $\omega = 1$, and $\Omega = 10$.

stable manifold. Due to the existence of the excitation, the phase trajectory moves around the stable equilibrium. The response is not divergent. If the stable equilibrium does not exist, the response will be rapidly divergent to infinity. Based on this idea, we labeled the location of x at a time point, which is long enough from the beginning. According to the existence of the labeled point, we estimate the existence of the stable equilibrium. Adopting this method, the bifurcation diagram is numerically computed in Fig. 5. If $F = 0$, the bifurcation diagram is continuous and of the transcritical type. Under different fractional-order α, this fact is verified in Fig. 5. Hence, the numerical simulation of the transcritical bifurcation in Fig. 5 coincides with its analytical prediction in Fig. 1. If $F \neq 0$, the bifurcation diagram is of the saddle-node type. The numerical results of the saddle-node bifurcation points approximately agree with the analytical results. Due to the existence of the high-frequency excitation, the response is always trying to deviate from the region of the stable manifold. As a consequence, it results that the numerical result is a little smaller than the analytical one. In a word, when the system parameter changes from negative to positive, the saddle-node bifurcation occurs twice. This fact can be verified by both analytical and numerical methods.

3.3 The High-Frequency Force Induced Saddle-Node Bifurcation. The saddle-node bifurcation diagram induced by the force amplitude F is shown in Fig. 6. With the increase of F, there is only once saddle-node bifurcation for a certain value of the fractional-order. It is different from the parameter μ induced saddle-node bifurcation in which there are two saddle-node bifurcations appearing when μ increases from negative to positive. Also in Fig. 6, we can see that the bifurcation point turns right gradually with the increase of the fractional-order α. When the parameter F passes through the bifurcation point, there is no equilibrium point any longer and the system will be rapidly divergent under the excitation.

Some phase trajectories under different simulation parameters are given in Fig. 7. To obtain each subplot, we let $F = 3$, 10, 20, and 40, respectively. The phase trajectories for $F = 3$ and $F = 10$ are shown in Fig. 7(a). However, for the case $F = 20$ and $F = 40$,
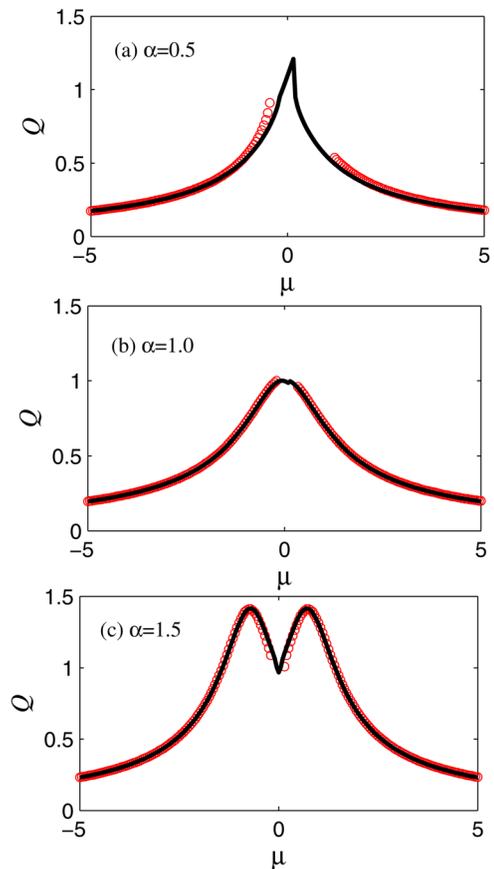

Fig. 11 The response amplitude Q versus the system parameter μ presents the resonance-like behavior. The continuous lines are the analytical predictions and the discrete points are the numerical results. The simulation parameters are $f = 0.1$, $\omega = 1$, $F = 1$, and $\Omega = 10$.

the phase trajectories do not appear in Fig. 7(a). It is because there is no stable equilibrium when $\alpha = 0.5$, $F = 20$, and $F = 40$, as shown in Fig. 6(a). Hence, there is no stable manifold existing for the two cases. It makes the response to increase rapidly to infinity under these simulation parameters. Due to the same reason, for the case $F = 10$, 20, and 40 in Fig. 7(b), for the case $F = 40$ in Figs. 7(c) and 7(d), the response is divergent and there is no phase trajectory. In Figs. 7(e) and 7(f), the phase trajectories exist for $F = 3$, 10, 20, and 40. It is because the stable equilibria always exist for these simulation values, as shown in Fig. 6. The phase trajectory is an assistant tool to judge the existence of the stable equilibrium.

In Fig. 8, the numerical prediction of the bifurcation point is clearly shown. When F passes through the bifurcation point, the response is divergent. The numerical results in this figure correspond with the analytical predictions in Fig. 6 approximately. In Fig. 8, the discontinuous property of the diagram is verified again. Both from Figs. 6 and 8, we find that the bifurcation point appears at a larger value of F for a larger value of the fractional-order α.

3.4 The Fractional-Order Induced Saddle-Node Bifurcation. In Figs. 9 and 10, the effect of the fractional-order α on the saddle-node bifurcation is shown analytically and numerically, respectively. With the increase of the fractional-order α, the stable branch of the equilibrium appears at the bifurcation point. Both from Figs. 9 and 10, the critical value of α corresponding to the bifurcation point turns larger with the increase of F. Hence, the fractional-order α is a key factor to induce the saddle-node bifurcation in Eq. (3). When other parameters are fixed, the equilibrium point is much more likely to exist for a large value of α. The fractional-order induced saddle-node bifurcation is in the supercritical case.

4 Nonlinear Response to the Low-Frequency Force

The response of the system to the low-frequency force can be quantified by the response amplitude Q, which is defined in Eq. (16). For numerical simulation, Q is computed by

$$Q = \sqrt{Q_{\sin}^2(\omega) + Q_{\cos}^2(\omega)}/f \quad (17)$$

where $Q_{\sin}(\omega)$ and $Q_{\cos}(\omega)$ are the Fourier coefficients

$$Q_{\sin}(\omega) = \frac{2}{rT}\int_0^{rT} x(t)\sin(\omega t)dt, \quad Q_{\cos}(\omega) = \frac{2}{rT}\int_0^{rT} x(t)\cos(\omega t)dt \quad (18)$$

Herein, $T = 2\pi/\omega$, r is a positive integer, which should be large enough, and $x(t)$ is the time series, which is directly calculated from the original equation.

If the parameter μ is a control parameter, then there is apparently a resonance-like peak in the $Q - \mu$ curve, as shown in Fig. 11. When $\alpha = 0.5$ and $\alpha = 1.0$, as shown in Figs. 11(a) and 11(b), respectively, the single resonance occurs when μ approaches to the origin for the two cases. When $\alpha = 1.5$, in Fig. 11(c), the double resonance occurs. There is a valley at the origin. The system parameter induced resonance in this figure is very similar to the vibrational resonance phenomenon in the fractional-order system [29]. Further, the analytical predictions agree with the numerical simulations, which justify the validity of the analysis in this paper. In this figure, we see that the resonance appears by adjusting the system parameter.
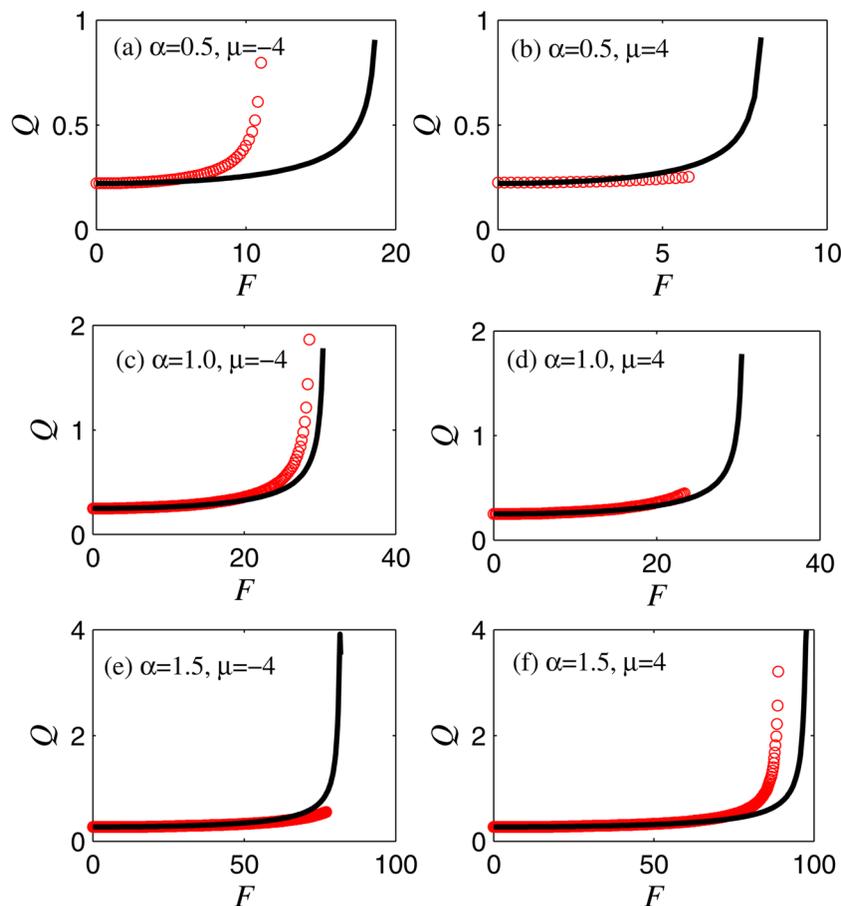

Fig. 12 The response amplitude Q versus the force amplitude F does not present the resonance-like behavior. The continuous lines are the analytical predictions and the discrete points are the numerical results. The simulation parameters are $f = 0.1$, $\omega = 0.5$, and $\Omega = 10$.
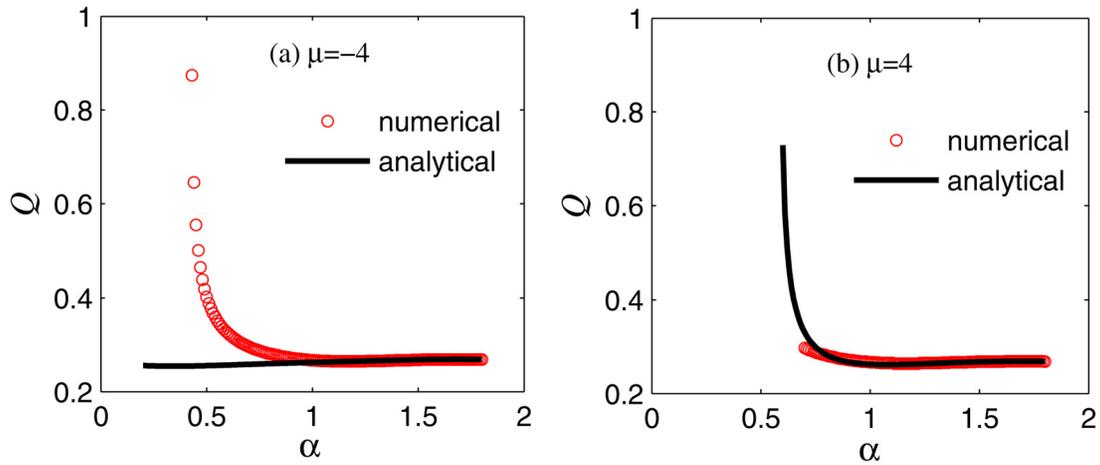
Fig. 13 The response amplitude Q versus the fractional-order α does not present the resonance-like behavior. The continuous lines are the analytical predictions and the discrete points are the numerical results. The simulation parameters are $f = 0.1$, $\omega = 0.5$, $F = 10$, and $\Omega = 10$.

In Fig. 12, the effect of the force amplitude F on the response amplitude Q is shown. Apparently, no vibrational resonance phenomenon appears. Specifically, with the increase of F, there is no resonance-like phenomenon occurring. The response amplitude will rise up to infinity with the increase of F. It is different from the dynamics behavior in the bistable systems [25,29,32,36–39]. In this figure, when other parameters are fixed, the response amplitude Q diverges at smaller F for smaller α. It is because X^*
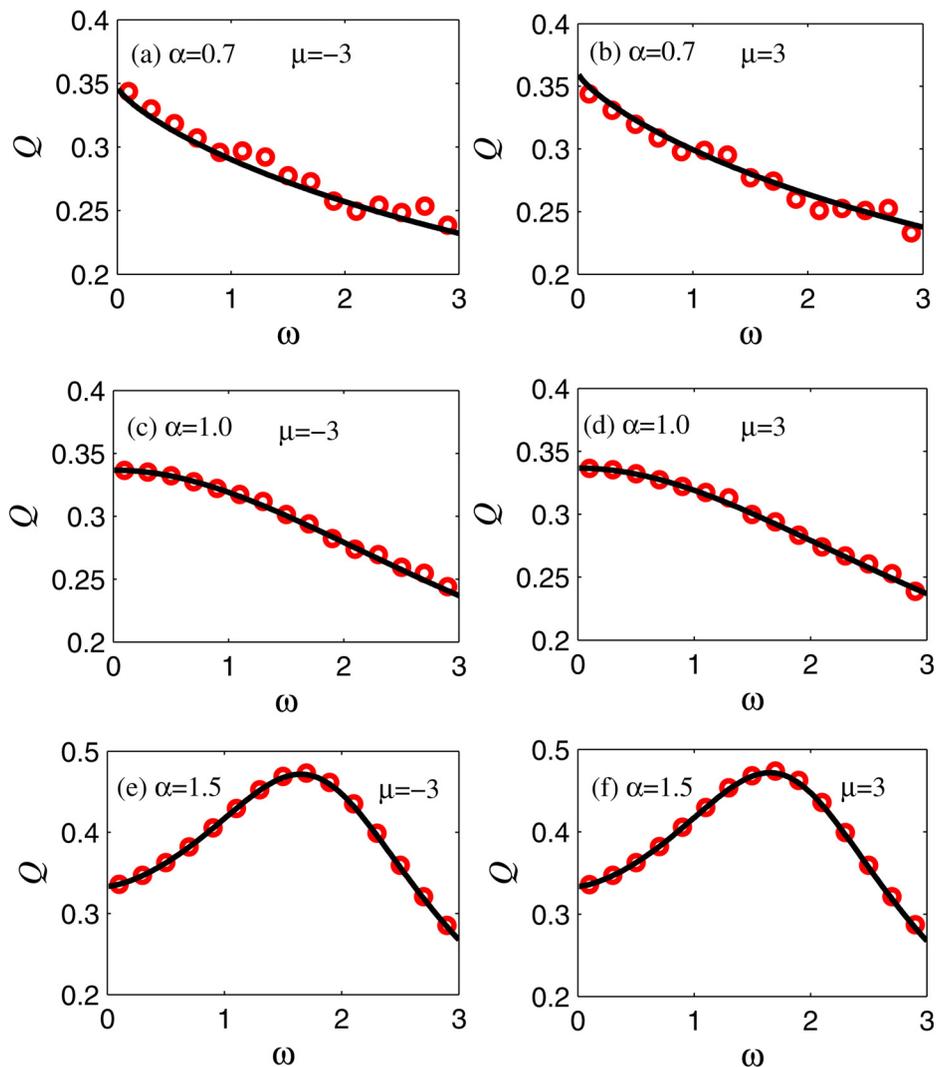

Fig. 14 The resonance behavior of Q versus the low-frequency ω depends on the fractional-order α. The continuous lines are the analytical predictions and the discrete points are the numerical results. The simulation parameters are $f = 0.1$, $F = 6$, and $\Omega = 20$.

vanishes at smaller F for smaller α, as shown in Fig. 6. This divergent phenomenon can also be seen from Fig. 8. It is difficult to realize the resonance-like behavior by adjusting the amplitude of the high-frequency force.

The effect of the factional-order α on the response amplitude Q is shown in Fig. 13. With the increase of α, the response amplitude Q decreases to a smaller value. To the contrary, at a smaller value of α, the response diverges. The nonlinear property of the response amplitude Q versus the fractional-order α is displayed. However, there is no resonance-like behavior in this figure.

In Fig. 14, the resonance dependence of the response amplitude Q on the low-frequency ω for fixed high-frequency force and fixed system parameter μ is illustrated. For the cases $\alpha = 0.7$ and $\alpha = 1.0$, there is no resonance behavior. For the case $\alpha = 1.5$, the resonance appears. Thus, we can control the resonance frequency by changing the value of the fractional-order.

5 Conclusions

In this work, the bifurcation behaviors and the response dynamics in a fractional-order oscillator is investigated. The bifurcation can be predicted by analytical and numerical methods. When there is no external excitation acting on the system, the system parameter will induce a transcritical bifurcation. If there is only one excitation, the transcritical bifurcation still exists and the phase trajectories will move around the stable equilibrium. If the system is excited by both a low- and a high-frequency force, the system parameter, the high-frequency, and the fractional-order will also induce bifurcations. However, due to the biasing effect of the high-frequency force, the transcritical bifurcation disappears, and the saddle-node bifurcation appears instead. For this case, the system parameter and the low-frequency will induce twice a saddle-node bifurcation. The amplitude of the high-frequency force and the fractional-order will induce once a saddle-node bifurcation only. As to the response amplitude to the low-frequency of the excitation, the system parameter and the low-frequency will induce the resonance-like behavior, but the high-frequency force and the fractional-order cannot induce the resonance-like behavior. We believe that the results shown in this paper might be useful for a better understanding of the bifurcation and resonance behaviors in the fractional-order systems.

References

[1] Torvik, P. J., and Bagley, R. L., 1984, "On the Appearance of the Fractional Derivative in the Behavior of Real Materials," ASME J. Appl. Mech., 51(2), pp. 294–298.
[2] Diethelm, K., and Freed, A. D., 1999, "On the Solution of Nonlinear Fractional-Order Differential Equations Used in the Modeling of Viscoplasticity," Scientific Computing in Chemical Engineering II, Springer, Berlin Heidelberg, Germany, pp. 217–224.
[3] Bagley, R. L., and Calico, R. A., 1991, "Fractional Order State Equations for the Control of Viscoelastically Damped Structures," J. Guid. Control Dyn., 14(2), pp. 304–311.
[4] Adolfsson, K., Enelund, M., and Olsson, P., 2005, "On the Fractional Order Model of Viscoelasticity," Mech. Time-Depend. Mater., 9(1), pp. 15–34.
[5] West, B. J., Bologna, M., and Grigolini, P., 2003, Physics of Fractal Operators, Springer, New York, pp. 235–270.
[6] Yang, F., and Zhu, K., 2011, "A Note on the Definition of Fractional Derivatives Applied in Rheology," Acta Mech. Sin., 27(6), pp. 866–876.
[7] Wu, G. C., Baleanu, D., and Zeng, S. D., 2014, "Discrete Chaos in Fractional Sine and Standard Maps," Phys. Lett. A, 378(5–6), pp. 484–487.
[8] Wu, G. C., and Baleanu, D., 2014, "Discrete Fractional Logistic Map and Its Chaos," Nonlinear Dyn., 75(1–2), pp. 283–287.
[9] Wu, G. C., and Baleanu, D., "Discrete Chaos in Fractional Delayed Logistic Maps," Nonlinear Dyn., (in press).
[10] Syta, A., Litak, G., Lenci, S., and Scheffler, M., 2014, "Chaotic Vibrations of the Duffing System With Fractional Damping," Chaos, 24(1), p. 013107.
[11] Cao, J., Ma, C., Xie, H., and Jiang, Z., 2010, "Nonlinear Dynamics of Duffing System With Fractional Order Damping," ASME J. Comput. Nonlinear Dyn., 5(4), p. 041012.
[12] Yang, J. H., Sanjuán, M. A. F., Xiang, W., and Zhu, H., 2013, "Pitchfork Bifurcation and Vibrational Resonance in a Fractional-Order Duffing Oscillator," Pramana, 81(6), pp. 943–957.
[13] Yang, J. H., Liu, H. G., and Cheng, G., 2013, "The Pitchfork Bifurcation and Vibrational Resonance in a Quintic Oscillator," Acta Phys. Sin., 62(18), p. 180503.
[14] El-Saka, H. A., Ahmed, E., Shehata, M. I., and El-Sayed, A. M. A., 2009, "On Stability, Persistence and Hopf Bifurcation of Fractional Order Dynamical System," Nonlinear Dyn., 56(1), pp. 121–126.
[15] Babakhani, A., Baleanu, D., and Khanbabaie, R., 2012, "Hopf Bifurcation for a Class of Fractional Differential Equations With Delay," Nonlinear Dyn., 69(3), pp. 721–729.
[16] Abdelouahab, M., Hamri, N., and Wang, J., 2012, "Hopf Bifurcation and Chaos in Fractional-Order Modified Hybrid Optical System," Nonlinear Dyn., 69(1–2), pp. 275–284.
[17] Sun, K., Wang, X., and Sprott, J. C., 2010, "Bifurcations and Chaos in Fractional-Order Simplified Lorenz System," Int. J. Bifurcation Chaos, 20(4), pp. 1209–1219.
[18] Guckenheimer, J., and Holmes, P., 2002, Nonlinear Oscillations, Dynamical Systems and Bifurcations of Vector Fields, Springer-Verlag, New York, pp. 117–165.
[19] Thomsen, J. J., 2003, Vibrations and Stability: Advanced Theory, Analysis, and Tools, Springer-Verlag, Berlin, Heidelberg, Germany.
[20] Medio, A., and Lines, M., 2001, Nonlinear Dynamics: A Primer, Cambridge University Press, Cambridge, pp. 133–148.
[21] Blekhman, I. I., 2000, Vibrational Mechanics: Nonlinear Dynamic Effects, General Approach, Applications, World Scientific, Singapore.
[22] Blekhman, I. I., 2003, Selected Topics in Vibrational Mechanics, World Scientific, Singapore.
[23] Monje, C. A., Chen, Y., Vinagre, B. M., Xue, D., and Feliu-Batlle, V., 2010, Fractional-Order Systems and Controls: Fundamentals and Applications, Springer, London, UK, pp. 10–12.
[24] Thomsen, J. J., 2002, "Some General Effects of Strong High-Frequency Excitation: Stiffening, Biasing, and Smoothening," J. Sound Vib., 253(4), pp. 807–831.
[25] Jeyakumari, S., Chinnathambi, V., Rajasekar, S., and Sanjuán, M. A. F., 2011, "Vibrational Resonance in an Asymmetric Duffing oscillator," Int. J. Bifurcation Chaos, 21(1), pp. 275–286.
[26] Thomsen, J. J., 1999, "Using Fast Vibrations to Quench Friction-Induced Oscillations," J. Sound Vib., 228(5), pp. 1079–1102.
[27] Jeevarathinam, C., Rajasekar, S., and Sanjuán, M. A. F., 2011, "Theory and Numerics of Vibrational Resonance in Duffing Oscillators With Time-Eelayed Feedback," Phys. Rev. E, 83(6), p. 066205.
[28] Yang, J. H., and Zhu, H., 2013, "Bifurcation and Resonance Induced by Fractional-Order Damping and Time Delay Feedback in a Duffing System," Commun. Nonlinear Sci. Num. Simul., 18(5), pp. 1316–1326.
[29] Yang, J. H., and Zhu, H., 2012, "Vibrational Resonance in Duffing Systems With Fractional-Order Damping," Chaos, 22(1), p. 013112.
[30] Borromeo, M., and Marchesoni, F., 2006, "Vibrational Ratchets," Phys. Rev. E, 73(1), p. 016142.
[31] Rajasekar, S., Abirami, K., and Sanjuán, M. A. F., 2011, "Novel Vibrational Resonance in Multistable Systems," Chaos, 21(3), p. 033106.
[32] Blekhman, I. I., and Landa, P. S., 2004, "Effect of Conjugate Resonances and Bifurcations Under the Biharmonic Excitation of a Pendulum With a Vibrating Suspension Axis," Dokl. Phys., 49(3), pp. 187–190.
[33] Tcherniak, D., 1999, "The Influence of Fast Excitation on a Continuous System," J. Sound Vib., 227(2), pp. 343–360.
[34] Hansen, M. H., 2000, "Effect of High-Frequency Excitation on Natural Frequencies of Spinning Discs," J. Sound Vib., 234(4), pp. 577–589.
[35] Jensen, J. S., 1997, "Fluid Transport due to Nonlinear Fluid–Structure Interaction," J. Fluid Struct., 11(3), pp. 327–344.
[36] Landa, P. S., and McClintock, P. V. E., 2000, "Vibrational Resonance," J. Phys. A: Math. Gen., 33(45), pp. L433–L438.
[37] Blekhman, I. I., and Landa, P. S., 2004, "Conjugate Resonances and Bifurcations in Nonlinear Systems Under Biharmonical Excitation," Int. J. Nonlinear Mech., 39(3), pp. 421–426.
[38] Chizhevsky, V. N., and Giacomelli, G., 2006, "Experimental and Theoretical Study of Vibrational Resonance in a Bistable System With Asymmetry," Phys. Rev. E, 73(2), p. 022103.
[39] Chizhevsky, V. N., 2008, "Analytical Study of Vibrational Resonance in an Overdamped Bistable Oscillator," Int. J. Bifurcation Chaos, 18(6), pp. 1767–1773.